This article can be cited before page numbers have been issued, to do this please use: C. Gu and L. Botto, *Soft Matter*, 2018, DOI: 10.1039/C7SM01912B.

Journal Name

ARTICLE TYPE

Cite this: DOI: 10.1039/xxxxxxxxxx

Buckling vs. particle desorption in a particle-covered drop subject to compressive surface stresses: a simulation study

Chuan Gu[a] and Lorenzo Botto[a*]

Received Date
Accepted Date

DOI: 10.1039/xxxxxxxxxx

www.rsc.org/journalname

Predicting the behaviour of particle-covered fluid interfaces under compression has implications in several fields. The surface-tension driven adhesion of particles to drops and bubbles is exploited for example to enhance the stability of foams and emulsion and develop new generation materials. When a particle-covered fluid interface is compressed, one can observe either smooth buckling or particle desorption from the interface. The microscopic mechanisms leading to the buckling-to-desorption transition are not fully understood. In this paper we simulate a spherical drop covered by a monolayer of spherical particles. The particle-covered interface is subject to time-dependent compressive surface stresses that mimic the slow deflation of the drop. The buckling-to-desorption transition depends in a non-trivial way on three non-dimensional parameters: the ratio Π_s/γ of particle-induced surface pressure and bare surface tension, the ratio a/R of particle and drop radii, and the parameter f characterising the strength of adhesion of the particle to the interface. Based on the insights from the simulations, we propose a configuration diagram describing the effect of these controlling parameters. We find that that particle desorption is highly correlated with a mechanical instability that produces small-scale undulations of the monolayer of the order of the particle size that grow when the surface pressure is sufficiently large. We argue that the large local curvature associated with these small undulations can produce large normal forces, enhancing the probability of desorption.

1 Introduction

Particles of intermediate wettability can strongly adhere to the surface of droplets or bubbles[2,3,4,5], forming a semi-solid "skin" that changes the mechanical and mass transport properties of the fluid interface. This modification can have macroscopic, leading-order effects. For example, the presence of the particles can improve the stability of foams and emulsions[6], slow down phase coarsening in multiphase mixtures[7], and alter the permeability of the fluid interface[4].

A measure of the ability of a solid particle to adhere to a fluid interface is the single-particle adsorption energy, *i.e.* the work required to remove a particle from a fluid interface in the absence of other particles. For chemically homogeneous particles residing on a flat fluid interface, the single-particle adsorption energy is given by $\Delta E = \pi\gamma a^2(1-|\cos\theta|)^2$[3], where a,γ and θ are the particle radius, the surface tension of the bare fluid interface and the contact angle, respectively. The single-particle adsorption energy is often compared to the thermal energy kT to determine whether

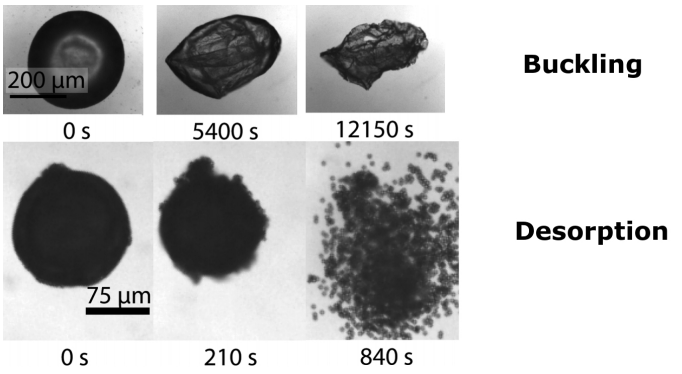

Fig. 1 Dissolving air bubbles covered with microparticles of different sizes. Top: buckling for $a/R = 0.0012$. Bottom: desorption for $a/R = 0.03$ (From Ref.[1]). The parameter a/R is the ratio between the radius of each particle and the radius of the bubble.

[a*] *Queen Mary University of London, School of Engineering and Materials Science, Mile End Road E1 4NS, London, UK. E-mail: l.botto@qmul.ac.uk*

† Electronic Supplementary Information (ESI) available: analysis of pressure difference across interface vs. surface pressure; dependence of surface pressure on particle size for linear inter-particle force model; effect of numerical parameter s on buckling time. See DOI: 10.1039/b000000x/

a particle will reside in the fluid interface or desorb. The typical argument, suggested by the literature on molecular surfactants, is that a particle can be assumed to be irreversibly attached to the fluid interface when $\Delta E \gg kT$ [2]. However, this argument does not take into account that the particles can be pushed out of the fluid interface by the interaction with other particles [1,8–10]. Such effect of particle desorption caused by inter-particle interactions and the work done by particle-induced surface stresses can in principle occur whenever the particle-covered interface is locally compressed due, *e.g.*, to a change in volume or shape of the region enclosed within the fluid interface [11,12].

An alternative outcome of the compression of a particle-covered interface is the occurrence of monolayer buckling (sometimes also referred to as crumpling in the literature). For particle-covered bubbles and drops subject to quasi-static deformations, buckling leads to the appearance of smooth wrinkles having amplitude and wavelength comparable to the drop or bubble radius R. The macroscopic appearance of buckled particle-covered drops and bubbles is similar to that of a buckled continuous shell, but the discrete nature of the particles makes the analogy valid only qualitatively. For example, the dependence of the buckling pressure on R for particle-covered drops and bubbles is different from the one expected from the classical theory of elastic spherical shells [13,14]. Identifying the parameters controlling the emergence of particle desorption instead of smooth buckling could open up interesting applications such as triggered particle release from coated bubbles for biomedical applications [1] or on-demand destabilisation of particle-stabilised foams.

Systematic experiments examining the transition between buckling and particle desorption in the limit of quasi-static deformations are limited to Langmuir trough experiments on flat particle-covered interfaces [9,10]. These investigations reveal that i) desorption is sensitive to local particle configurations and "defects" in the monolayer packing, and ii) the contact angle of the particle plays an important role in the buckling-to-desorption transition as it determines how strongly the particle is attached to the fluid interface. Experimental studies on buckling and collapse of drops or bubbles covered with non-cohesive particle monolayers under slow, quasi-steady compression of the particle layer have mostly focused on the change in morphology of the particle-covered interface and how such morphology depends on the pressure difference Δp across the interface [13–18]. As for an elastic shell, the shape of the particle-laden interface changes at a critical value of Δp (and therefore, equivalently, at a critical value of the average surface pressure of the particle-laden interface). The critical value of Δp producing a non-spherical interface and the post-buckling morphology was found to depend on a/R [13,14,16]: a transition between a morphology presenting smooth wrinkles and a morphology presenting flat facets occurs for a/R in the neighbourhood of 0.1 [13,16]. In these studies particle expulsion was not the subject of the investigation. However, it was noticed that for values of Δp just above the critical value the particle layer displayed small, $O(a)$, displacements about the average position of the fluid interface [13,14]. This small-scale feature was found to be important to explain the effective resistance of the particle layer to lateral compression as well as its buckling behaviour.

Simulations of buckling of particle-covered drops or bubbles in which the discrete nature of the particles is captured are a few and limited to relatively large values of a/R. A well-resolved simulation is that of Abkarian et al. [16], who used Surface Evolver to simulate a drop or bubble (gas compressibility effects were not discussed in the paper) covered with spherical particles for $a/R \simeq 0.1$. These authors found that, in keeping with experimental results, for $a/R \simeq 0.1$ the particle-laden drop/bubble presented flat facets when Δp was increased above a critical threshold (here we take Δp to denote the difference in pressure between the outside and the inside of the interface). The extremely high resolution employed in this simulation allowed the authors to prove that the as the drop/bubble volume was reduced, the fluid interface between the particles started to curve inward after near maximum packing was achieved. The change in morphology of drops covered with homogeneous and Janus particles for $a/R = 0.1$ and subject to volume reduction was studied by Dissipative Particle Dynamics in Ref. [19]. These simulations include Brownian fluctuations. It was found that for chemically-homogenous spherical particles, the volume reduction of the drop leads to a particle-covered drop that looked macroscopically spherical, except for the formation of small scale layering of the particles and the presence of localised out-of-plane particle displacements. It was also found that the inclusion of chemical heterogeneity of the particle surfaces had a dramatic effect on the post-buckling shape of the drop. A two-dimensional phase-field simulation of a drop covered by slightly non-spherical particles, for a/R roughly equal to 0.15, suggest that when the pressure difference across the interface $\Delta p = 0$, the particle-laden drop is in a metastable configuration and many different drop shapes are possible depending on the history of deformation [20]. To the best of our knowledge no simulation work has explored the range $a/R = 0.01 - 0.1$.

A potentially important parameter controlling the buckling-to-desorption transition is the size ratio a/R. Partial evidence of this effect is given in figure 1, from Ref. [1]. This figure shows an experiment in which a bubble covered by a (nominally) monodispersed monolayer of hydrophilic polystyrene microparticles is slowly compressed. The surface compression is obtained by increasing the solubility of the gas in the liquid [1], which produces an outward flux of gas and a reduction in bubble volume. In the case illustrated in the top panel, in which $a/R = 0.0012$, the compression of the monolayer produced by the shrinkage of the bubble gives rise to pure buckling. In the case illustrated in the bottom panel, in which $a/R = 0.03$ the particles instead are seen to desorb from the surface of the bubble, eventually accumulating at the the bottom of the container (for $t = 840s$). While several factors could potentially play a role in the observed transition (e.g. differences in contact angle, polydispersity, etc.), the size ratio could be important even in the situation in which the other factors are negligible.

In this article, we study the transition from buckling to desorption by modelling a spherical drop covered by a monodispersed monolayer of spherical particles and subject to compressive surface stresses, focusing on the range $a/R = 0.01 - 0.1$. The simulations are carried out with FIPI [21], a numerical method that we have developed recently. In the simulations the strength of

interparticle repulsive force is modulated in time to determine compressive surface stresses. The time-dependence is sufficiently slow that the deformation is quasi-static. For numerical reasons, the particle interactions are modelled by soft repulsive forces, but the main results are applicable to the limit "steric" repulsion due to granular contacts. We follow the time-dependent morphology of the fluid interface and of the particle monolayer, and examine the local particle dynamics, by changing the following non-dimensional parameters: the size ratio between the particle and the drop a/R, the non-dimensional parameter f quantifying the strength of adhesion of the particles to the fluid interface (this parameter is independent of the particle size) and the non-dimensional ratio between the surface pressure Π_s and the bare surface tension γ. Our simulations suggest that desorption can be a result of a small scale monolayer shape instability which may not be easily observed in experiments, pointing to the importance of microscopic rearrangement on the macroscopic dynamics.

The computational model proposed in the current paper is meant to mimic the driven deflation of a particle-covered drop due to e.g. to mass removal from a portion of the drop boundary[13], evaporation or osmotic pressure differences (as in dissolution or osmotic shock experiments), in the case quasi-static limit of extremely small deformation rates and therefore negligible effect of fluid stresses on the interface shape. If compressibility effects are neglected, our results are also valid for bubbles. Relevant experiments are those in which the volume of a drop or bubble decreases due to mass transfer to the external phase driven by undersaturation. Examples include buckling of nanoparticle-coated droplets upon addition of undersaturated continuous phase[22] and destabilisation beyond dissolution arrest of particle-coated bubbles when undersaturation is induced by a change in temperature[1].

A reason for the focus of previous simulations on relatively large values of a/R is the extremely large grid resolution required to capture accurately the small interfacial deformations between the particles. Explore realistic values of a/R (significantly smaller than 0.1) while exploring the parameter space reasonably well requires accepting a partial resolution of interfacial distortions at the particle level. This is the approach we have taken in the current article. The results are a first step towards more accurate simulations.

Ours appears to be the first systematic investigation of the transition between buckling and desorption using a simulation. Because in our work the rate of drop deformation is small (quasi-static deformation), viscous stresses do not play a role in setting the morphology of the interface. Provided that incompressibility and gravitational effects are comparatively small in comparison to effects due to interfacial mechanics, the result presented in the current article could thus be equally applicable to particle-covered droplets and particle-covered bubbles.

2 Computational Model

The simulations were performed with the Fast Interface Particle Interaction (FIPI) method[21]. FIPI is a mesoscale simulation method for particle-interface interaction problems that enables to simulate a large number of particles interacting with fluid interfaces of complex morphology. The method has shown to accurately capture particle-induced interfacial stresses[21]. FIPI couples a standard convective Cahn-Hilliard equation to a momentum equation for the fluid modified to account for the forces exerted by the particles on the fluid and on the fluid interface. The use of a phase-field formulation is not an essential feature of the FIPI method. In principle, FIPI can be adapted to any method that treats surface tension effects by amending the right-hand side of the Navier-Stokes equation with forcing terms.

The Cahn-Hilliard equation for the phase field variable ϕ reads

$$\frac{\partial \phi}{\partial t} + \mathbf{u}\cdot\nabla\phi = M\nabla^2\xi, \tag{1}$$

where $\xi = \frac{\lambda}{\varepsilon^2}\left(\phi^3-\phi\right) - \lambda\nabla^2\phi$ is the chemical potential, λ is a numerical parameter proportional to the surface tension, and ε is a parameter defining the thickness of the fluid interface and M is a mobility parameter. All these parameters are standard in Cahn-Hilliard formulations[23]. The bare surface tension is calculated as $\gamma = \frac{2\sqrt{2}}{3}\frac{\lambda}{\varepsilon}$. This parameter characterises the isotropic tension in the fluid interface in the absence of the particles[21].

The convective term in the Cahn-Hilliard equation couples the shape of the interface to the Navier-Stokes equation, which in turn accounts for the presence of the particles. This term is therefore essential.

We assume that the fluids inside and outside of the droplet have identical viscosity μ, and operate in the low-Reynolds number limit for which fluid inertia can be neglected.The phase field in Eq. (1) is advected with the fluid velocity $\mathbf{u}$. This field is calculated by solving an augmented Stokes equation at each time step :

$$-\nabla p + \mu\nabla^2\mathbf{u} + \xi\nabla\phi + \sum_{i=1}^{N}\mathbf{F}_i\delta(\mathbf{x}_i) = 0. \tag{2}$$

The term $\xi\nabla\phi$ is the volumetric force produced by the surface tension of the bare fluid interface (i.e., in the absence of the particles). The presence of the particles is accounted for by the summation term, which runs over the N particles present in the computational domain. This term involves delta forces of strength $\mathbf{F}_i$ applied at the center $\mathbf{x}_i$ of each particle. The summation term represents the forces exerted by the particles on the bulk fluid and on the fluid interface. Neglecting particle inertia, and modelling the hydrodynamic drag using Stokes' drag law, the particle equation of motion reads

$$-6\pi a\mu\mathbf{u}_p^{(i)} = \mathbf{F}_{pi}^{(i)} + \mathbf{F}_{pp}^{(i)}, \tag{3}$$

where a is the particle radius, $\mathbf{u}_p^{(i)}$ is the particle velocity, $\mathbf{F}_{pi}^{(i)}$ is the capillary adhesion force exert by the fluid interface on the particle and $\mathbf{F}_{pp}^{(i)}$ is the force on particle (i) due to particle-particle interactions with neighbouring particles. In Stokes' law we have neglected the fluid velocity at the particle position, as we have found that the self-induced fluid velocity due to the particle forcing term in (2) can sometimes affect the particle desorption when the normal force on the particle is high (corresponding to high surface pressure values). Ways to mitigate this effect are under investigation.

For the particle-particle interaction term we have adopted the

following linear model :

$$\mathbf{F}_{pp}^{(ij)} = \begin{cases} -k(r-r_c)\mathbf{n}_{ij}, & \text{if } r < r_c \\ \mathbf{0}, & \text{if } r > r_c \end{cases} \quad (4)$$

where $\mathbf{F}_{pp}^{(ij)}$ is the force on particle i due to particle j, $\mathbf{n}_{ij}$ is the unit vector along the line connecting the centres of particles i and j (pointing towards j), k is a spring constant quantifying the strength of the interaction (with units of force per unit length) and r_c is a cut-off length. Linear models are commonly employed in granular flow simulations to model contact forces between nominally rigid particles[24–26]. An ideal hard-core repulsion corresponds to the limits $k \to \infty$ and $r_c \to 2a$.

Our original plan with the simulation was to consider hard-core repulsion, to mimic steric repulsion between rigid spherical particles (granular "contact"). However, resolving the particle dynamics with sharply decaying repulsive forces requires extremely small computational time steps (even in simulations were the fluid interface is not present and the Navier-Stokes equation is not solved). Taking into account the need to simulate a reasonably wide parameter range while keeping the simulation cost manageable, we have therefore settled for a soft potential, setting $r_c = 5a$ and using finite values of k. Using a soft potential does not alter the essential physics (although it affects somewhat the degree of lateral order in the interface). This is because buckling and particle expulsion occur when the lateral and normal forces reach threshold values, independently from the specific law of dependence between $\mathbf{F}_{pp}^{(ij)}$ and r (see also discussion in Ref. [16]).

Setting r_c to a value significantly larger than $2a$ has two further advantages. Firstly, we can simulate the effects of a large surface pressure without reaching maximum surface packing (which for $r_c = 2a$ is about 0.92). This choice enabled us to run with a smaller number of particles and therefore a smaller computational overhead. Secondly, using a soft repulsion allows the freedom to lower the spring constant. This in turn permits the use of larger time steps. A crucial advantage of using a linear particle-particle interaction model is that for a linear model the surface pressure depend on the surface fraction ϕ_s, but is independent of a/R (the proof is provided in the supporting information S2). Therefore one can explore the effect of changing a/R while keeping the surface pressure constant. Non-linear models do not have this feature.

The attachment force of each particle to the fluid interface is parameterised as

$$\mathbf{F}_{pi}^{(i)} = \begin{cases} f\pi\gamma\mathbf{d}, & \text{if } d \le d_{max} \\ \mathbf{0}, & \text{if } d > d_{max} \end{cases}, \quad (5)$$

where f is a non-dimensional parameter, $\mathbf{d}$ is the minimum distance vector pointing from the particle centre to the zero level set of the phase field variable ϕ, $d = |\mathbf{d}|$ and d_{max} is the value of d for which the particle desorbs from the fluid interface. The level set indicates the position of the interface, including the capillary disturbance produced by particle i A linear law $\propto \gamma d$ is expected from dimensional considerations. Linear laws where the displacement includes also the capillary bridge holding the particle to the interface have been shown to be approximately valid almost up to the point of desorption[27–29] (where non-linear effects start becoming important). The length of the capillary bridge at rupture can be a few times a[27–29]. However, d is the distance of the particle centre from the surface $\phi = 0$, not from the undisturbed fluid interface. Hence we have taken $d_{max} = a$. In the current version of FIPI, the contact-angle dependent shift of the particle centre of mass with respect to the surface $\phi = 0$ is not accounted for directly, but only through f.

In our modelling approach, all the information about the strength of attachment of the particle to the interface is lumped into f. Physically, this parameters depends on the contact angle, surface roughness, surface chemical heterogeneity, and on the ratio of particle size to the local curvature of the interface[28–30]. An approximate mapping between f and the contact angle that would ensure that (5) recovers know adsorption energies can be obtained by calculating the work of desorption corresponding to (5), $\Delta E = \frac{1}{2} f\pi\gamma a^2$, and comparing the result to single-particle adsorption energy expressions.

Using $\Delta E = \pi\gamma a^2(1-|\cos\theta|)^2$ [2] valid for isolated, chemically-homogeneous spherical particles on a flat surface we obtain $f = 2(1-|\cos\theta|)^2$. Taking θ to be the contact angle measured between the solid surface and the fluid interface on the outside of the drop, we get $f = 0$ for $\theta = 0°$ (particle residing in the outer liquid and just touching the interface) and $f = 2$ for $\theta = 90°$ (particle straddling the interface in a neutral-wetting configuration). The expression $\Delta E = \pi\gamma a^2(1-|\cos\theta|)^2$ characterises the energy of desorption of a particle in the most favourable liquid region. It is thus not valid to quantify the effect of values of $\theta > 90°$ (particle mostly immersed in the inner liquid) when desorption is forced to occur towards the outer liquid. In this case, one should use the expression $\Delta E = \pi\gamma a^2(1-\cos\theta)^2$. Values $f > 2$ are thus physically possible (see detailed discussion in Ref. [3]). In our problem values $f > 2$ would correspond to particles mostly immersed in the inner liquid being forced to desorb in the outer liquid by repulsive inter-particle forces. Analytical results for single particles on curved interfaces of curvature $1/R$ show that for $\theta = 90°$ the work to detach a particle from an interface for $a/R = 0.01$ is roughly 2 times higher than what predicted by the expression $\Delta E = \pi\gamma a^2(1-|\cos\theta|)^2$ [29]. The mapping between f and θ should be adjusted accordingly, and would lead to $f \simeq 4$ for $\theta = 90°$. It should be noted that the work to detach the particles appearing in the literature typically include the work to deform the capillary bridge that extends between the particle and the undisturbed fluid interface. Theoretical bounds for f and an accurate analysis of the dependence of f as defined in (5) on the contact angle for smooth chemically-homogeneous spheres are under development and will be presented in a forthcoming publications.

To summarise, the linear expression (5) is a good approximation of the microscopic physics of particle attachment to fluid interfaces. What is incompletely known is the mapping between f and particle parameters (contact angle, surface roughness, surface chemical heterogeneity, etc.) for a particle surrounded by other particles in a particle monolayer. However, in the current work we are content with exploring the effect of changing f on the transition between buckling and desorption, regardless of the

exact features of this mapping.

Regarding the accuracy of the method, and its ability to capture experimental features, the following considerations should be kept in mind. FIPI replaces the effect of the particle on the interface with the normal capillary force exerted by the particle on the interface. This is an essential feature of the interaction with particles to fluid interface. However, higher-order modes of the capillary traction on the fluid interface, which would give rise to small undulations in the interface very near the particle are not captured beyond the monopole level. Even with fully-resolved codes capturing accurately these small features requires a very large resolution near the particle. Currently, only methods that mesh the fluid interface as Surface Evolver can ensure an accurate resolution of these features, and only for systems with not too many particles. Furthermore, capturing in simulation particle surface effects such as contact line pinning, which have been proven to be important in experiments [14], poses great conceptual and technical challenges even considering one or few particles. In our model, contact line pinning would affect the value of the parameter f, likely making it larger for a given contact angle.

For a fixed Cahn number $Cn = \varepsilon/L$, where L is the domain size, the non-dimensional parameter controlling the spreading of the diffuse interface is $s = \frac{\sqrt{M\mu}}{\varepsilon}$. This parameter is the ratio of the length scale $\sqrt{M\mu}$ characterising the diffusion of the chemical potential ξ to the thickness ε of the fluid interface [31–33]. Choosing s requires addressing competing requirements. Large values of s damp the fluid velocity near the fluid interface, which in turn leads to a loss of small scale features in the distribution of ϕ. Small values of s leave the fluid interface vulnerable to thinning or thickening under straining flows [31]. As a compromise, in our simulations we used $s = 0.5$, unless specified otherwise. This value has been chosen based on numerical tests with particle-covered drops subject to compressive surface stresses: in these tests for s in the neighborhood of 0.5 the fluid interface thickness was observed to be roughly constant in time and to have approximately the hyperbolic tangent profile expected near equilibrium. Following other authors [32,34] we set the Cahn number to $Cn = 0.013$. The ratio dx/ε of the mesh size to the interface thickness was $2\sqrt{2}/3 \simeq 0.94$ in all simulations. This choice gives about 6 grid nodes across the region where ϕ varies from -0.963 and 0.963.

2.1 Simulation procedure

The simulation domain is a cubic box of side $L = 3\pi$. Periodic boundary conditions are enforced along the three orthogonal directions. The governing equations are solved with a standard Fourier-spectral method, eliminating the pressure p from the momentum equation by using the incompressibility condition [35]. We discretise the domain using 80 nodes in each orthogonal direction. The fluids inside and outside of the droplet have the same dynamic viscosity μ. At the start of simulations a spherical droplet with radius $R = 0.8\pi$ is placed at the centre of the domain. The particles are initially distributed uniformly on the surface of the droplet, by applying a uniform probability distribution to a spherical coordinate system [36]. The initial particle surface fraction $\phi_s = \frac{N}{4}\frac{a^2}{R^2}$ is equal to 0.5 in all the simulations.

The surface pressure overaged over the surface of the particle-laden drop is calculated as [21]

$$\Pi_s = \frac{1}{2A}\sum_{m>n} F_i^{mn} l_i^{mn}, \tag{6}$$

where A is the fluid interface surface area, F_i^{mn} is the modulus of the interparticle force between particle m and particle n and l_i^{mn} is the corresponding interparticle separation. We calculate the area by using the software Paraview. This software calculates the surface area of the iso-surface $\phi = 0$ from the distribution of the phase-field variable. Paraview is also used to compute the local interface curvature. From Π_s we calculate the total packing energy E_p of a particle monolayer as

$$E_p = 2\Pi_s A. \tag{7}$$

During the shrinkage of a particle-laden drop or bubble, buckling or desorption occurs when the surface pressure reaches a threshold value as the surface area decreases [8,22,37]. Simulating an increase in surface pressure by reducing the drop volume by removing mass from the inside of the drop is possible, and we have explored this possibility in preliminary work. However, this approach has several disadvantages. First of all, when using a computational box of finite size the simulated flow velocity is inevitably affected by the conditions at the outer boundaries. With a cubic box and periodic boundary conditions, for example, the computed velocity field is not spherically symmetric and for an initially spherical drop this leads to a loss of spherical symmetry in the phase field distribution that is not due to a buckling instability. Secondly, identifying the rate of volume reduction for which the process is quasi-steady is challenging. A further disadvantage of increasing the surface pressure by reducing the drop volume is that it is difficult to compare different simulation results for different values of a/R. For example, when comparing two simulations for the same initial drop radius but different particle size, small particles will give buckling for a later time than larger particles so the droplet radius at the moment of buckling will be different in the two cases.

We have therefore opted to keep the drop volume constant, and change the surface pressure by varying k in equation (4). Two modes of variation of k with time are used (Figure 2):

- Mode 1: k is kept to a constant value k_0 throughout the simulation, where k_0 is chosen so that Π_s is larger than γ. To allow the particles to reorganise themselves on the fluid interface while maintaining a spherical drop, in the initial part of the simulation, i.e. for $t < t_1^i$, , we disable the forcing parameter in the Stokes equation (2). For $t_1^i < t < t_1^{end}$, where t_1^{end} is the simulation end time, the forcing term $\mathbf{F}_i$ is enabled. In this two-way coupling stage the drop shape is affected by the particle distribution.

- Mode 2: We slowly increase k from 0 to 2γ, using for simplicity a linear variation. The slow variation of k enables the particles to reorganise themselves on the surface of the drop while the surface pressure builds up. In mode 2, the forcing term in equation (2) is enabled at all times. As far as

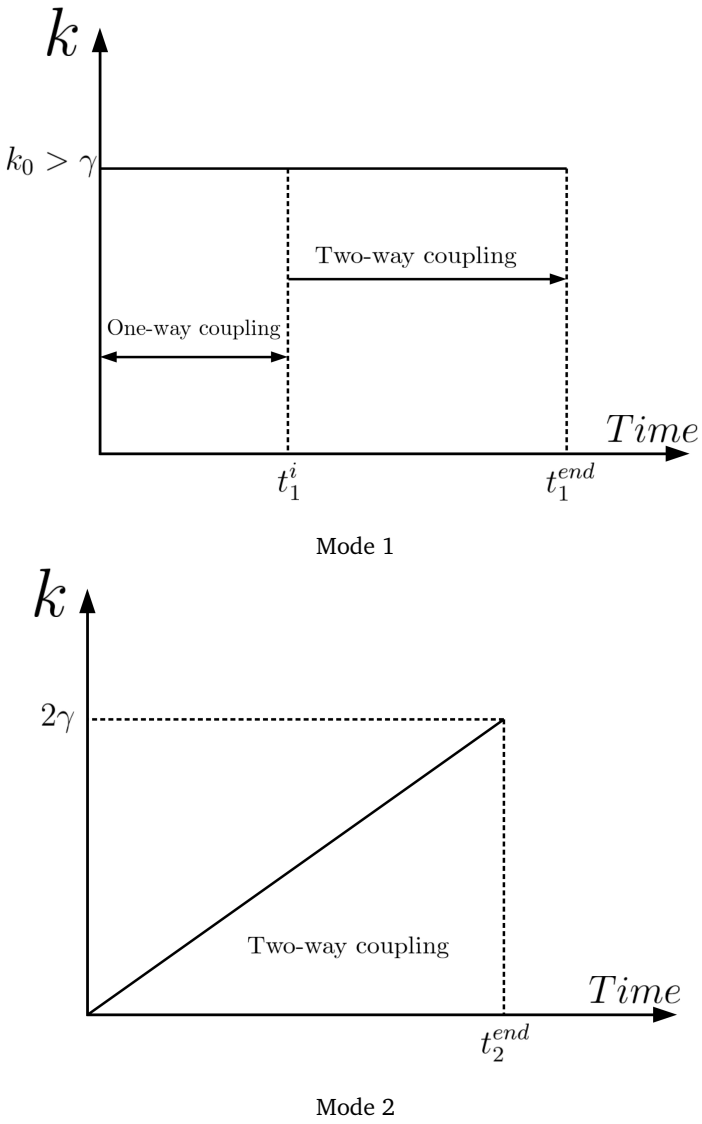

Fig. 2 Modes of variation with time of the inter-particle force parameter k (eq. 4). For the simulations investigating the time evolution for pure buckling we used mode 1. For the simulations investigating the effect of f and a/R we used mode 2.

buckling and desorption are concerned, increasing k in time is physically equivalent to shrinking the drop, but we avoid the numerical artefacts mentioned above (see the Supporting Information for a numerical test showing the equivalence of a volume reduction and an increase in surface pressure in the context of our problem).

For the simulations investigating the time evolution for pure buckling (in the absence of desorption) we used mode 1. For these simulations our aim was to evaluate the effect of Π_s on the emergence of buckling. Thus, it was important to keep k, and thus Π_s, constant. The investigations on the effect of f and a/R were instead carried out by using mode 2.

3 Results

Time evolution of drop morphology for pure buckling (no desorption). Threshold surface pressure for buckling. Figure 3 shows the time evolution of the drop shape and of the particle distribution for an initial surface pressure $\Pi_s = 1.5\gamma$. As we are here interested in the case in which desorption is absent, we set f to a large value, $f = 10$, to prevent any significant displacement of the particles from the fluid interface. At the beginning of the simulation the particles are randomly distributed on the surface of the drop (Figure 3A). Following an initial transient, in which the particles rearrange themselves on the surface of the drop, a regular particle microstructure characterised by a dominant hexagonal arrangement emerges (Figure 3B)[38]. After some time the drop loses its spherical shape and buckles (Figures 3C and D).

To quantify the precise time instant at which the buckling instability develops, we have examined the total packing energy of the monolayer E_p (eq. 7) and the corresponding drop surface area A. The time evolution of E_p and A, and the time derivative of these quantities, are shown in Figures 4a and b. The labels A, B, C, and D indicate the time instants corresponding to the drop morphologies of Figure 3.

Owing to the initial reorganisation of the particles, from time instant A to B the packing energy decreases, but the surface area remains unchanged. This is expected, because between time instants A and B the one-way coupling regime ($t < t_1$ in Fig. 2), which gives a spherical drop shape, is used. At time instant B, the two-way coupling is switched on. A buckling process characterised by a simultaneous decrease in the packing energy and an increase in the surface area begins. The time derivative of the surface area dA'/dt' (primes denote non-dimensional quantities) reaches its maximum approximately in correspondence to the time instant C. The decrease in E_p and the increase in A are apparently synchronised, with the peak value of dA'/dt' just slightly lagging behind that of dE_p'/dt'. At the time instant D, both E_p' and A' reach a steady state. Interestingly, both ratios converge exactly to the same value. This is due to the fact that the steady state is achieved when $\Pi_s = \gamma$ (by definition $E_p' = \frac{\Pi_s}{\gamma}\frac{A}{A_0}$, hence $E_p' = A'$ as $\Pi_s \to \gamma$).

We define the buckling time T_b as the time instant for which dA'/dt' has a peak. We have calculated T_b for different values of Π_s/γ. The results are shown in Figure 5.

The first observation is that all the data points lie in the region $\Pi_s > \gamma$. For $\Pi_s < \gamma$, the particle-covered interface is in a state of tension, and therefore buckling cannot occur. For $\Pi_s > \gamma$ the buckling time diverges as Π_s approaches γ from above, and decrease as Π_s increases. These features can be rationalised with a simple model. For $\Pi_s > \gamma$ the particle-covered interface is subject to a compressive surface stress of magnitude $\Pi_s - \gamma$. Equating the capillary force $\sim (\Pi_s - \gamma)R$ acting on the drop surface to the viscous force $\sim \mu UR$ resisting the motion of the interface, the characteristic normal interfacial velocity U during the evolution of the buckling instability is of $O((\Pi_s - \gamma)/\mu)$. Estimating T_b as the time taken by the interface to move a distance comparable to R yields

$$T_b \simeq \frac{R\mu}{\Pi_s - \gamma}. \tag{8}$$

As seen in figure 5, equation (5) describes the trend of the simulation data remarkably well with no fitting parameters.

View Article Online
DOI: 10.1039/C7SM01912B

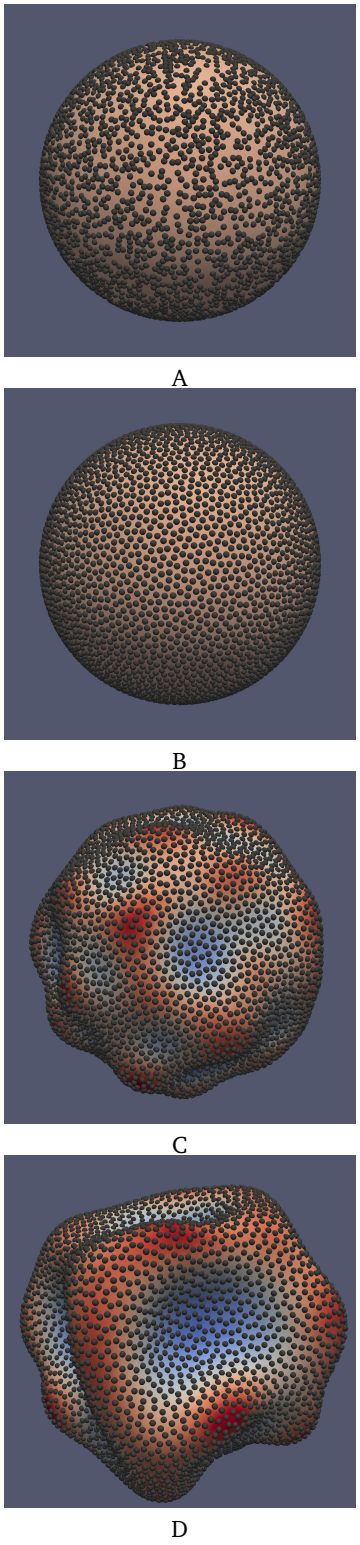

Fig. 3 Time evolution of drop morphology and particle distribution for $f = 10$, $a/R = 0.02$ and $\Pi_s/\gamma = 1.5$. The labels A, B, C, and D correspond to different times (compare with Fig. 4).

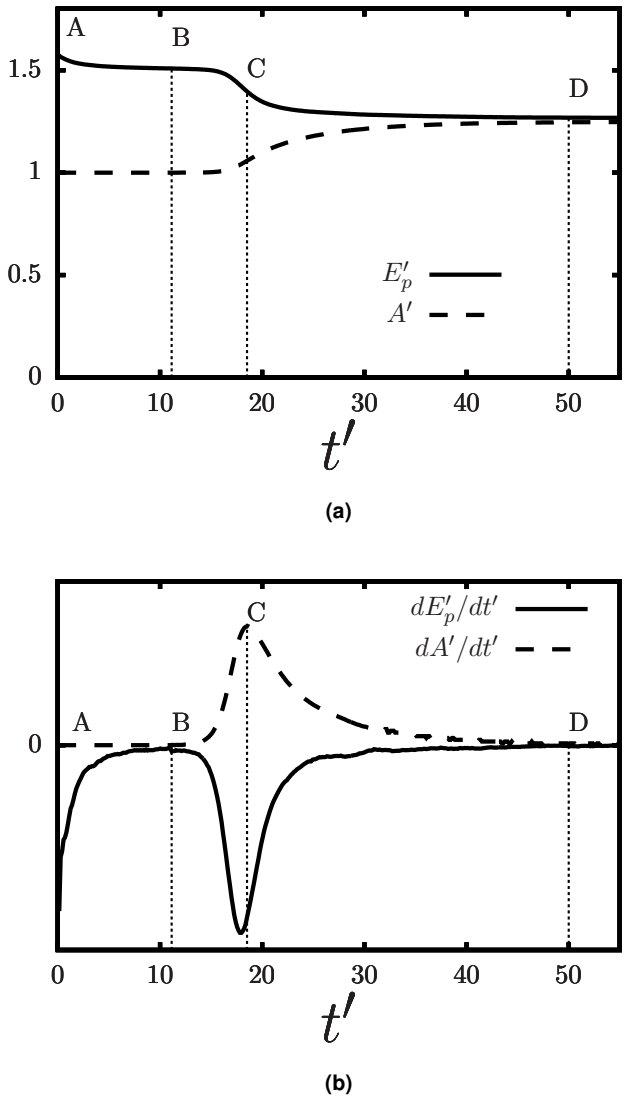

Fig. 4 (a) Time history of the non-dimensional packing energy and surface area. (b) Time history of the non-dimensional rates of change of E_p and A with respect to time. Primes indicate dimensionless variables: $t' = t\gamma/(R\mu)$, $A' = A/A_0$ and $E'_p = E_p/(2A_0\gamma)$, where A_0 is the initial drop surface area

Expression (8) shows that buckling can be an extremely slow process when Π_s is only slightly larger than γ. This observation is crucial for simulation studies. When simulating particle-laden drops or bubbles, one may have to carry out extremely long simulations to identify the onset of buckling with precision, as we have learned through direct experience. A drop, for example, may be declared not to buckle, when in fact the simulation has just not been run for a sufficiently long time. In our work, we have used eq. (5) as an important practical guideline to choose the duration of the simulations.

We have found that T_b converges accurately to the value predicted by equation (8) as the numerical parameter $s \to$ to 0 while keeping the fluid interface thickness ε constant. This result, which is related to numerical aspects of the phase-field method, is presented in the Supporting Information.

Effect of non-dimensional adhesion strength. In this section we examine the effect of the parameter f appearing in the particle-interface interaction model (5). This non-dimensional

View Article Online
DOI: 10.1039/C7SM01912B

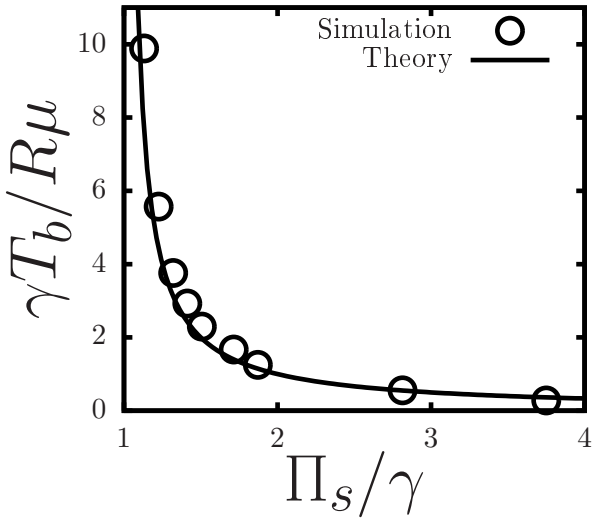

Fig. 5 Normalised buckling time vs. normalised initial surface pressure for $f = 10.0$. The solid line is the proposed model equation (8). The numerical parameter s is here set to 0.01.

quantity is proportional to the work necessary to remove a particle from the fluid interface, normalised by the capillary energy scale γa^2. It can also be interpreted as the work of adhesion of the particle monolayer to the fluid interface normalised with the surface tension. Indeed, the energy associated to N particle-interface capillary bonds distributed over an area A is $E_{tot} = N\frac{1}{2}f\pi a^2\gamma$, thus the work of adhesion is $\Gamma = n_s\frac{1}{2}f\pi a^2\gamma$ where $n_s = N/A$ is the particle surface number density. Introducing the surface area fraction $\phi_s = n_s\pi a^2$, we have $\frac{\Gamma}{\gamma} = \frac{1}{2}f\phi_s$. For identical spheres near maximum packing, the surface fraction is close to 1 ($\phi_s \simeq 0.92$[39]), thus $\frac{\Gamma}{\gamma} \simeq \frac{1}{2}f$.

The effect of changing f on the drop morphology is illustrated in Figure 6. The figure shows the shape of the drop and the corresponding particle distribution for selected times. In this figure f is varied from 1 to 4, two limits that are representative of weak and strong adhesion when f is mapped to the contact angle (see discussion in Sec. 2 to understand why we can set $f > 2$).

For $f = 1.0$ the particles are seen to desorb collectively from the fluid interface for non-dimensional time $t' < 209$. Uniform desorption of nanoparticles upon pendant drop compression was reported in the experiment of Ref.[8]. In that experiment the desorbed particles formed a thin halo adjacent to the drop surface. The halo slowly diffused outwards owing to Brownian motion. The particles eventually were swept by gravity towards the drop's bottom apex. In our simulations Brownian forces and gravity are not accounted for, so the particles remain close to the fluid interface after desorption. In Fig. 6a the particle layer appear to be diffused. This effect is simply due to the repulsion between the desorbed particles and the particles that are just undergoing desorption.

For intermediate adhesion strength, $f = 2$, no desorption is observed. The particle-covered fluid interface buckles, producing smooth wrinkles having a characteristic wavelength $\lambda \sim R$. For

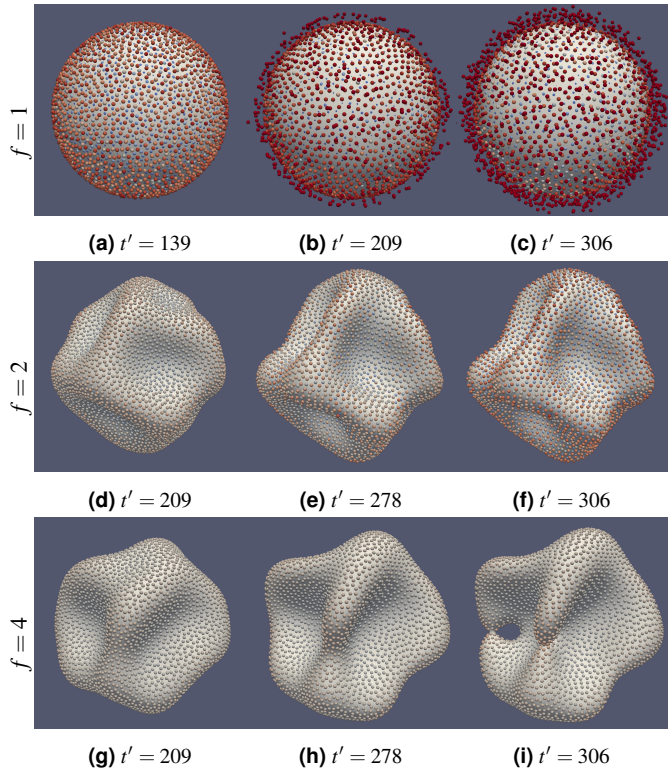

Fig. 6 Time evolution of the monolayer morphology for $a/R = 0.02$, $s = 0.5$ and different values of f. The particles are colored according to their signed distance from the fluid interface (red: outside of the drop; blue: inside of the drop; grey: embedded in the fluid interface).

larger adhesion strength, $f = 4$, the fluid interface buckles creating wrinkles qualitatively similar to those obtained for $f = 2$. A notable difference between the simulations for $f = 2$ and $f = 4$ is that for $f = 4$ the ridge of one of the surface folds breaks up locally (figure 6i). This breakup is likely due to the larger out-of-plane particle displacement allowed by smaller values of f.

Figure 7 provides a detailed view of the structure of the particle monolayer for $f = 1$ and $f = 4$. For $f = 4$ the adhesion between the particles and the fluid interface is strong. As a consequence the particles form a smooth monolayer that conforms closely to the fluid interface. For $f = 1$ the displacement of the particles from the fluid interface is instead larger. Neighbouring particles tend to reside on different sides of the fluid interface, forming small-scale undulations of amplitude $\sim a$ having characteristic width ℓ also comparable to a. We define this type of particle monolayer structure, characterised by small-wavelength small-amplitude out-of-plane particle displacement of the particles, *particle-scale monolayer undulations*. Desorption appears to be highly correlated with the emergence of this feature.

Small-amplitude out-of-plane particle displacements were also reported in recent experiments[13,14]. In the experiments with particle-covered bubbles of Ref.[14], particle-scale monolayer undulations were analysed with the help of a simple mathematical model. The model showed particle-scale undulations to be due to a small-wavelength mode of buckling, where the mechanical work performed by the surface pressure is balanced by the restoring elastic force $\sim \gamma a$ associated with the microscopic out-of-plane

View Article Online
DOI: 10.1039/C7SM01912B

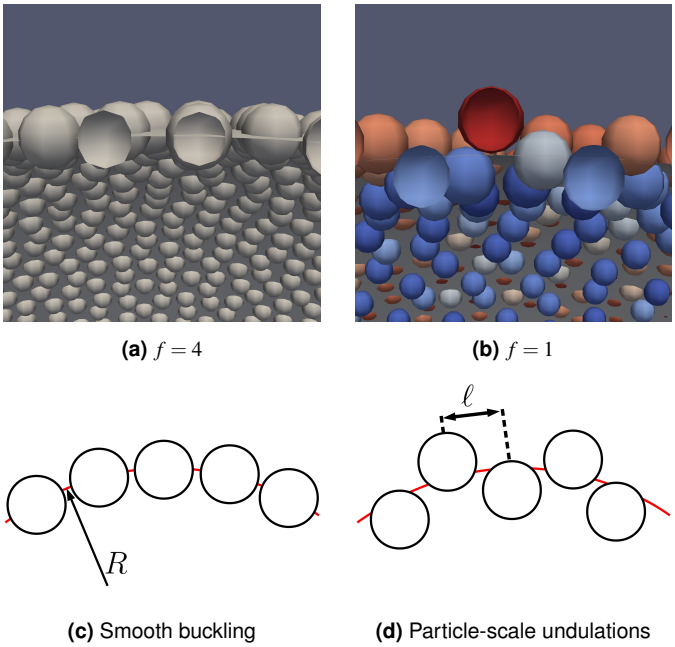

Fig. 7 Top: Enlarged views of monolayer configuration for $t' = 139$. The case $f = 1$ (fig. b) is the enlarged view of fig. 6a, focusing on the near-interface region. The meaning of the colours is as in fig. 6. Bottom: schematics of monolayer configurations corresponding to the simulation results of the top panel.

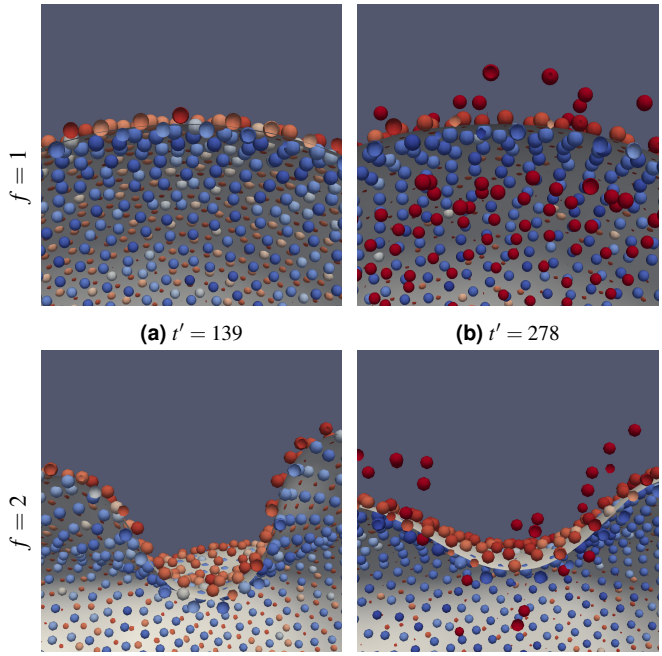

Fig. 8 Enlarged views of particle desorption events for different values of f and $a/R = 0.02$. The panels on the left and on the right refer to before and after desorption, respectively. For the particles bound to the interface, the meaning of the colours is as in fig. 6. Desorbed particles are coloured in dark red.

displacement of the particles. In the experiments with particle-covered drops of Ref.[13], "accordion patterns" of amplitude $\sim a$ in the particle monolayer were also described. The origin of the accordion patters was assumed to be small differences in particle size or contact angle between neighbouring particles. The surface pressure would be responsible for amplifying the initial out-of-plane displacement. This effect was indicated as a source of compressional elasticity of the monolayer near maximum packing.

The visualisations of figure 8 compare particle monolayer configurations before and after desorption for $f = 1$ and $f = 2$. These visualisations reveal that the particle monolayers display particle-scale undulations both before and after desorption. When $f = 1$, the particle monolayer is undulated at small scales without the fluid interface showing signatures of "large-scale" ($\sim R$) buckling. For $f = 2$, the particle monolayer produced particle-scale undulations only after the fluid interface had buckled significantly. The emergence of particle-scale undulations thus does not necessary follow from "large-scale" buckling, as particle-scale undulations can be superimposed onto a spherical or a buckled interface.

A strong correlation between particle-scale undulations and desorption is expected from consideration of the magnitude of the force exerted on a given particle in the direction normal to the fluid interface. This normal force is due to the lateral forces exerted by neighbouring particles. For a particle residing on a monolayer having local curvature $\mathscr{C}$, simple geometric arguments[13] enable to estimate the normal force on each particle as

$$F \simeq \frac{1}{2} N_c F_t a \mathscr{C} \qquad (9)$$

where N_c is the local coordination number and $F_t \simeq 2\pi\Pi_s a$ is the average tangential inter-particle force (in the derivation we have assumed $a\mathscr{C} \ll 1$ to obtain the dominant-order scaling). For a buckled monolayer, the observed wavelength $\lambda \sim R$ gives $F \simeq \frac{1}{2} N_c F_t \frac{a}{R}$. For a monolayer displaying particle-scale undulations - whether long-wavelength buckling occurs or not - the observed wavelength $\lambda \sim \ell$ gives $F \simeq \frac{1}{2} N_c F_t \frac{a}{\ell}$ to leading order. Recalling that $\ell \sim a$, the local normal force acting *locally* on the particles in the case of particle-scale undulations is thus $O(R/a)$ larger than for buckling. Because $a \ll R$, the normal force in the case of a monolayer presenting particle-scale undulations can thus be much larger, for the same value of the surface pressure, than in the case of a monolayer presenting smooth folds. The coupling between normal force and curvature is thus a mechanism that predicts enhanced probability of desorption as a/R increases.

Effect of size ratio. The visualisations in figure 9 show the effect of changing a/R on the drop morphology for $a/R = 0.01$, 0.04 and 0.08. A morphological transition occurs as a/R is increased, from a buckled drop shape for $a/R = 0.01$ to an almost spherical drop shape for 0.08. This qualitative observation is confirmed in figure 10, where we plot the sphericity parameter $\Psi = \frac{\pi^{\frac{1}{3}}(6V)^{\frac{2}{3}}}{A}$ as a function of a/R (V is the volume of the region comprised within the fluid interface and A the surface area of this region). The sphericity parameter is defined so that the larger the deviation from a spherical shape, the smaller the value of Ψ. A perfectly spherical shape corresponds to $\Psi = 1$.

The critical range of values of a/R for which the transition occurs, and how strong the dependence of Ψ on a/R is, depend

sensitively on f. For $f = 2$ a transition from an almost spherical ($\Psi \simeq 0.95$) to a non-spherical shape occurs for a/R in the range $0.03 - 0.05$. As f increases, the transition becomes less sharp, the maximum value of Ψ is reduced, and the critical range of values of a/R for which the most marked change in Ψ occurs shifts to the right. The possibility of observing of a spherical shape despite the surface pressure value $\Pi_s > \gamma$ is easy to explain. For relatively small values of f, the particles can release the surface stress by moving slightly outwards towards larger value of d. This displacement reduces the surface pressure below the buckling value $\Pi_s = \gamma$, hence the drop maintains a spherical shape. Of course, this effect is only possible if Π_s is only slightly larger than γ. However, we have found from the simulations that values of Π_s significantly larger than γ are difficult to obtain when particle-scale undulations take place, because the particles tend to desorb before such relatively large surface pressure values are reached.

The results in figure 9 and 10 give an indication of the overall shape of the drop, but do not characterise the displacement of the particle monolayer surface from the fluid interface. To address this point, we show in figure 11 the mean value $\langle d \rangle$ and standard deviation $d_{std} = \left(\left\langle (d - \langle d \rangle)^2 \right\rangle \right)^{1/2}$ of the out-of-plane displacement d. These statistics are computed by averaging, for a fixed time $t\gamma/(R\mu) = 278$, over all the particles in the monolayer.

Figure 11a shows that the mean value of the displacement increases with a/R. Equation (9) indicates that a linear relation holds between the average value of F and the average value of $\mathscr{C}$, which in turn would suggest $\frac{\langle d \rangle}{a} \propto a/R$ (the restoring capillary force in our model is linear in the displacement). A linear relation between $\frac{\langle d \rangle}{a}$ and a/R indeed holds, although approximately, suggesting the validity of eq. (9) in an average sense.

The standard deviation of the displacement also increases with a/R (figure 11b). This effect is stronger for $f = 2$ than for $f = 4$, so it cannot be attributed to $\sim R$ buckling. It is the manifestation of the appearance of small-scale undulations in the particle monolayer.

Interestingly, the amplitude of the particle-scale undulations, as measured by d_{std}/a, appear to increase with a/R. Thin elastic sheets on curved substrates develop buckling patterns whose amplitude and spatial distribution depend on the substrate curvature[40]. From a continuum perspective, a particle-covered drop can be viewed as an incompressible thin sheet (the particle monolayer) adhered to a soft curved surface (the drop), so a dependence of the amplitude and wavelength of the buckling pattern on the curvature of the drop is conceivable.

In figure 12a we examine effect of changing a/R on the time evolution of the non-dimensional surface area $A' = A/A_0$. We consider $a/R = 0.03$, 0.04 and 0.05. This is the range of values of a/R for which the largest variation in the sphericity parameter and d_{std} is observed. For $t' < 200$, roughly, A' is constant. For this range of values of t' the inter-particle force parameter k increases, following the linear variation of mode 2, but because the surface pressure does not exceed the buckling threshold the drop remains spherical. For $t' > 200$, A' increases, indicating that $\Pi_s > \gamma$. The non-dimensional surface area decreases after reaching a maximum that depends on a/R. This decrease is due to

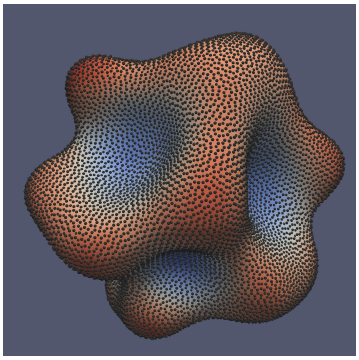

(a) $a/R = 0.01$

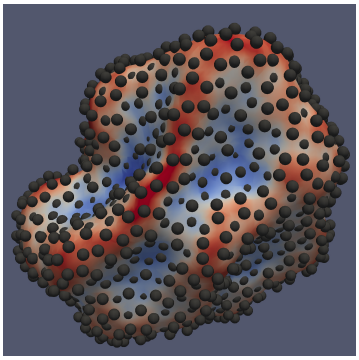

(b) $a/R = 0.04$

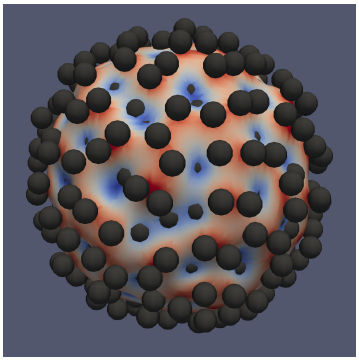

(c) $a/R = 0.08$

Fig. 9 Surface morphology for different values of a/R and $f = 2.0$. The time instant is $t\gamma/(R\mu) = 278$. The fluid interface is coloured according to its local curvature.

View Article Online
DOI: 10.1039/C7SM01912B

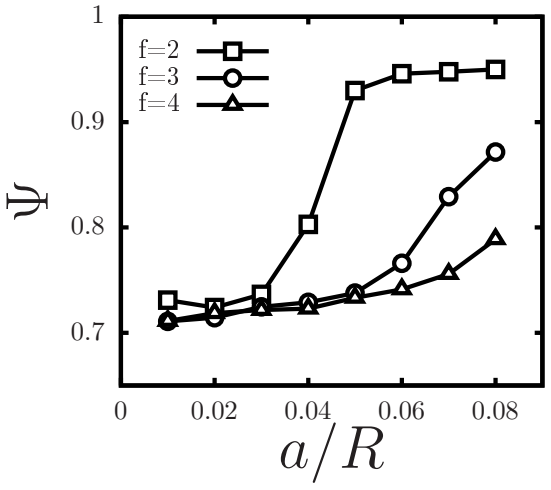

Fig. 10 Sphericity parameter as a function of a/R for different value of f and $t\gamma/(R\mu) = 278$.

particle desorption, which enables the drop to slowly recover the original spherical shape.

The visualisations of figure 12b show the drop shape and the monolayer configuration for the time instant for which A' has a peak. These figures show that the monolayer displays particle-scale undulations before desorption (red and blue colours refer to particles inside and outside the monolayer).

Although figure 12b and others presented in this paper do not strictly speaking prove a causality relation between particle-scale monolayer undulations and desorption, a strong correlation between these events appear to exist. A particle-level mechanisms exists. For a fixed value of Π_s/γ, particle-scale monolayer undulations increases the normal force on each particle due to local particle monolayer curvature effects, and this makes particle expulsion more likely.

4 Discussion

The simulation results presented in the previous sections suggest a complex dependence of the drop morphology and desorption dynamics on the non-dimensional parameters Π_s/γ, a/R and f, of which we have explored only a few selected values. In figure 13 we propose a configuration diagram that could help understand this dependence for a broader range of parameter values.

For buckling to occur the surface pressure induced by the particles must be larger than the bare surface tension γ (Figure 13a). This is true whatever the value of f. Buckling for values of Π_s smaller than γ has been reported for Langmuir trough experiments, but this effect has been ascribed to cohesiveness (which implies attractive inter-particle interactions, which are absent in our simulation) or to experimental difficulties in measuring the "true" surface pressure[10]. These difficulties are associated to many factors, including the fact that in Langmuir trough experiments the deformation is uni-directional, the surface pressure probe can disturb the surface displacement field, and the film can deform plastically.

The possible non-trivial outcomes of interface compression for

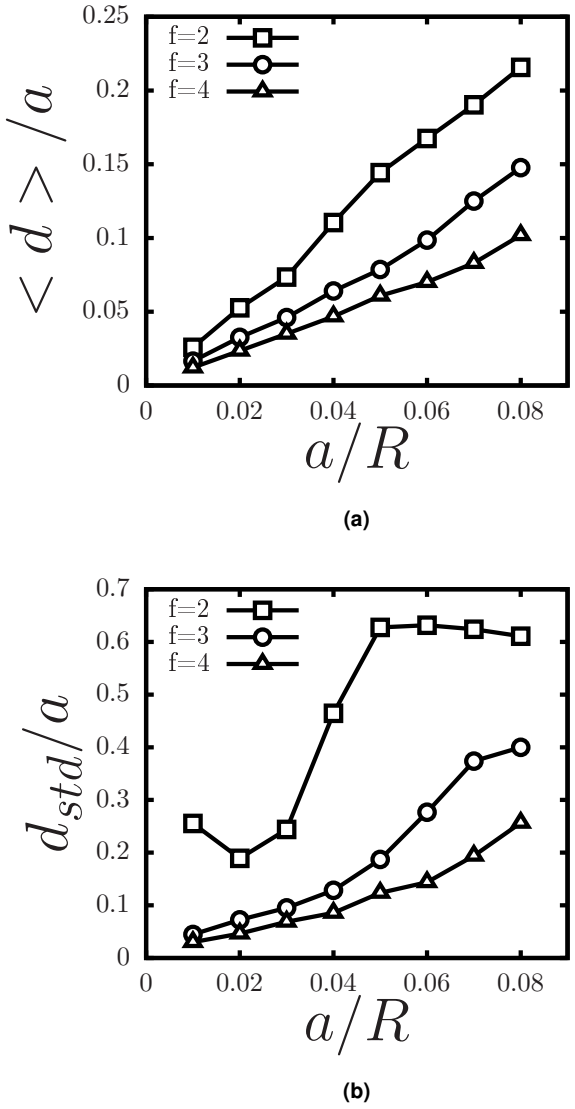

Fig. 11 Statistics of the out-of-plane displacement field d for $t\gamma/(R\mu) = 278$: (a) average; (b) standard deviation.

$\Pi_s < \gamma$ are particle-scale undulations in the monolayer or particle desorption. Desorption tend to occur when f is relatively small (see e.g. the uniform desorption of figure 6), because in this case the particles are very weakly attached to the fluid interface. Particle-scale undulations in the monolayer can occur for intermediate values of f. In this case, even though Π_s is smaller than γ the surface pressure can be sufficiently large to push the particles slightly out of the plane of the fluid interface. Particle-scale monolayer undulations tend to be negligible for large values of f when $\Pi_s < \gamma$. In this case the particle-covered drop remains spherical and the particle monolayer conforms closely to the spherical drop surface.

For $\Pi_s > \gamma$, two limiting behaviours separated by an intermediate regime can arise. Particle desorption takes place for "small" values of f. Pure buckling takes place for "large" values of f (in this case the monolayer is strongly bound to the fluid interface, so the surface pressure can only be released by out-of-plane

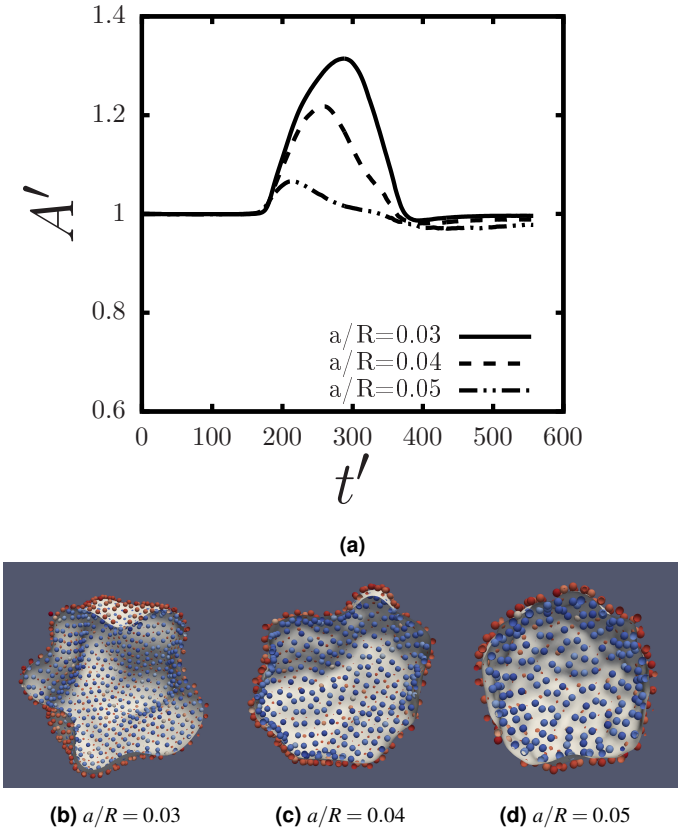

Fig. 12 (a) Time evolution of the normalised surface area $A' = A/A_0$ for different values of a/R and $f = 2.0$. The surface area is normalised by its initial value A_0. Time is normalised by the capillary time scale $t' = t\gamma/(R\mu)$. (b)-(d) Cross-sectional views of particle monolayer and fluid interface for different values of a/R. For each value of a/R, the time instant chosen correspond to just before the onset of desorption. Particles are coloured according to their signed distances from the fluid interface.

buckling of the particle-covered fluid interface). An intermediate behaviour characterised by smooth buckling superimposed on particle-scale monolayer undulations tend to occur. The diffuse transition region corresponding to this intermediate behaviour is indicated in yellow in Fig. 13. In the transition region f is not small enough to give particle desorption, but is sufficiently small to allow a significant particle displacement from the fluid interface.

As a surface pressure is increased for a fixed intermediate value of f, first particle-scale undulations appear (the yellow region is transversed) and then surface desorption occurs. Therefore, particle-scale undulations are a precursor to desorption in a process in which the surface pressure is increased.

The range of critical values of f separating desorption from pure buckling should somewhat depend on the surface pressure. Equation (9) suggests that the critical value of the normal force giving desorption, $f\gamma a$, is reached for $f \sim \frac{\Pi_s}{\gamma}\frac{a}{R}$. This estimate suggests a linear relation between f and Π_s in the transition region (this estimate assumes uniform interface curvature, and is thus just a rough approximation). In the absence of more information, we indicate the transition region as a diffuse region around a line in the $\Pi_s - f$ plane.

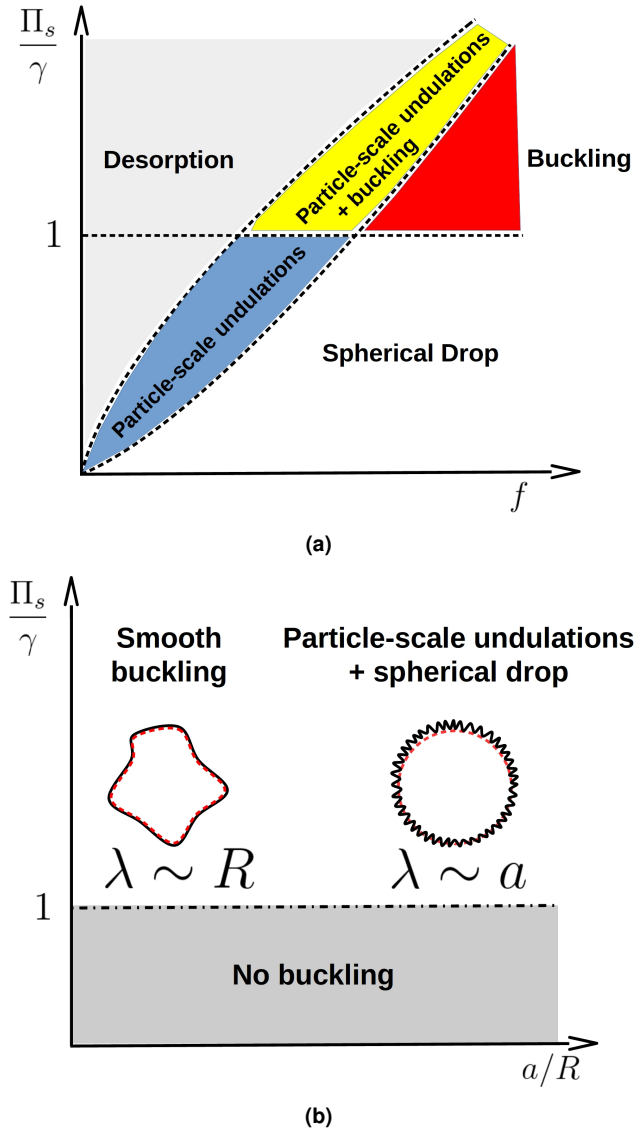

Fig. 13 Configurational diagrams of the qualitative dependence of the monolayer configuration on: (a) Π_s/γ and f, for intermediate and small values of a/R ; (b) Π_s/γ and a/R, for intermediate and large values of f. In (b) the continuous line (black) represents the particle monolayer and the dashed line (red) represents the fluid interface.

Figure 6 suggests a significant morphological transition for f between 1 and 2. Assuming $\Delta E = \pi\gamma a^2(1-|\cos\theta|)^2$, this range of values for f correspond to a relatively small change in contact angle, between 72° and 90°. This result suggests that different experiments with slightly different contact angles could give widely different outcomes when one examines the occurrence of buckling versus desorption.

For $\Pi_s > \gamma$ the particle monolayer displays different surface patterns depending on the value a/R (Figure 13b). In the case of "small" values of a/R, the simulations suggest a pure buckling pattern characterised by long-wavelength $\lambda \sim R$ folds. For "large" values of a/R the overall shape of the drop is spherical, and the monolayer displays particle-scale undulations with a characteristic wavelength $\lambda \sim a$ (as in Fig. 9c). A mixed behaviour (not illustrated in Figure 13b) may occur for intermediate values of a/R, whereby particle-scale monolayer undulations are accompanied by smooth buckling. This physical picture is characteristic of intermediate and large values of f. For small values of f the particles will desorb and the drop will remain spherical.

Unlike in the Surface Evolver simulation of Abkarian et al.[16] in our simulation we do not observe faceting. An explanation is the different in size ratio: their simulations focus on $a/R \simeq 0.1$ ($a/R \sim 0.13$ in their paper), while we considered much smaller size ratios (up to $a/R \leq 0.08$). Finite-size particle effects on capillarity, which are important when a/R is relatively large, are incompletely resolved in our model. In FIPI the effect of each particles on the fluid interface is replaced by a force, thus small-scale undulation of the interface near the particles tend to be smoothened out. In addition, the FIPI method is plagued by numerical instabilities when $a/R > 0.1$ and the surface pressure is relatively large so we were not able to explore the large a/R range.

If the desorption process involves many neighbouring particles simultaneously, the detachment of a particle monolayer from a fluid interface is akin to a buckling-induced delamination between two continuous sheets. The difficulty in applying continuum-level results[41–43] to particle desorption is the granular nature of the particle monolayer, which makes the desorption dynamics sensitive to the presence of defects, and the stress in the monolayer non-uniform and difficult to predict.

5 Conclusions

We have presented simulations with the FIPI method[21] of the compression of a particle-covered drop to understand the parameters affecting the change in morphology of the particle monolayer and of the fluid interface, and the conditions leading to particle desorption. The simulations are analysed as a function of the non-dimensional capillary adhesion strength f, the particle-to-drop size ratio a/R and the ratio Π_s/γ between the particle-induced surface pressure and the bare surface tension. The qualitative dependence on these parameters suggested by the simulations is illustrated in figure 13 and discussed in Sec. 4.

A general conclusion from our observation is that particle desorption is always associated to relatively low values of f. This conclusion agrees with the results of Langmuir trough experiments on planar interfaces[9,10]. In experiments, low values of f are the result of contact angles values for which the particle resides mostly in the subphase. While it could be assumed that contact angles for which the particle resides mostly in the superphase could also give desorption, gravity can keep the particles close to the interface[10], reducing the probability of observing desorption. In our model gravity is absent, but the curvature of the drop introduces an asymmetry, causing the particles to be expelled mostly from the interior of the drop outwards.

Particle-scale undulations are important to trigger desorption. For a given surface pressure, the normal force due to smooth buckling is $F \propto 1/R$. In contrast, particle scale undulations give $F \propto 1/a \gg 1/R$. The large local curvature associated to particle-scale undulations thus produces large normal forces, increasing the probability of desorption.

Our simulations are carried out under ideal conditions: the particles have identical size, identical wetting properties (f is constant), and can slide freely past each other because of the absence of tangential inter-particle interactions. As a consequence, under a spherically symmetric compression of the drop (mimicked in out simulation through an increase in Π_s), the properties of a point in the monolayer surface are identical in an average sense to those of any other point. The uniformity of particle properties and the isotropic geometry of the drop lead to a relatively uniform and isotropic small-scale surface pattern. In contrast, under realistic experimental conditions it is expected that particle size polydispersity, small differences in contact angle, and non-uniform inter-particle interactions, will lead to a more inhomogeneous particle-scale undulation pattern.

A significant contribution of our work is the exploration of curvature effects. We found that relatively large values of a/R favour the emergence of particle-scale monolayer undulations , which in turn tend to produce desorption when the surface pressure increases. Small values of a/R tend to produce pure buckling. This result is in qualitative agreement with the observations accompanying figure 1.

The results of the current work are valid for quasi-static situations. Experiments report buckling and particle expulsion in highly-dynamic situations in which time-dependent pressure fields change the shape of particle-covered bubbles[1,44]. In these situations both the particle and the fluid inertia are important. Particle inertia provides an additional normal force on each particle which adds to the normal force due to repulsive particle-particle interactions discussed in the current paper. The motion of the fluid will affect the particle positions and potentially compress locally the particle monolayer (due to changes in surface area owing to hydrodynamic stresses, or due to converging surface velocity streamlines[45]). The relevance of our work to these situations need to be examined carefully, as the conclusion will depend on the relative importance of interfacial and fluid forces.

In addition to the parameters explored in the current work, a variety of additional factors - some of them already mentioned - could play a role in the transition between buckling and desorption, such as polydispersity in particle size, differences in contact angle, the presence of inter-particle adhesion or the effect of gravity. Our results suggest that these factors, while potentially important, are not necessary to observe a transition. With FIPI we have carried out some initial numerical experiments introducing inter-

particle attraction and tangential inter-particle forces in addition to short range repulsion, to mimic cohesive particle layers. These initial tests reveal that the system's behaviour is much more complex than for pure repulsion, because with attractive interactions the surface stress can become non-uniform even when the drop is spherical. This features makes the theoretical analysis of the problem extremely challenging. Exploring cohesive monolayers is a worthwhile pursuit for future investigations.

6 Acknowledgement

We thank V. Garbin, Imperial College, for suggesting us to work on the problem of buckling vs. desorption and for sharing her experimental insights. We thank A. Striolo and F. Sicard (University College London) for useful discussions. Financial support from the European Community through Career Integration Grant FLOWMAT "Flow and Capillarity in Material Science" (No. 618335) is acknowledged.

Conflict of interest

There are no conflicts to declare.

References

1 V. Poulichet and V. Garbin, *Langmuir*, 2015, **31**, 12035–12042.
2 B. P. Binks, *Current Opinion in Colloid & Interface Science*, 2002, **7**, 21–41.
3 B. P. Binks and T. S. Horozov, *Colloidal particles at liquid interfaces*, Cambridge University Press, 2006.
4 A. Dinsmore, M. F. Hsu, M. Nikolaides, M. Marquez, A. Bausch and D. Weitz, *Science*, 2002, **298**, 1006–1009.
5 V. Garbin, J. C. Crocker and K. J. Stebe, *Journal of colloid and interface science*, 2012, **387**, 1–11.
6 E. Dickinson, *Current Opinion in Colloid & Interface Science*, 2010, **15**, 40–49.
7 K. Stratford, R. Adhikari, I. Pagonabarraga, J.-C. Desplat and M. E. Cates, *Science*, 2005, **309**, 2198–2201.
8 V. Garbin, J. C. Crocker and K. J. Stebe, *Langmuir*, 2011, **28**, 1663–1667.
9 S. Razavi, K. D. Cao, B. Lin, K. Y. C. Lee, R. S. Tu and I. Kretzschmar, *Langmuir*, 2015, **31**, 7764–7775.
10 S. Bordács, A. Agod and Z. Hórvölgyi, *Langmuir*, 2006, **22**, 6944–6950.
11 A. B. Subramaniam, C. Mejean, M. Abkarian and H. A. Stone, *Langmuir*, 2006, **22**, 5986–5990.
12 V. Poulichet and V. Garbin, *Proceedings of the National Academy of Sciences*, 2015, **112**, 5932–5937.
13 O. Pitois, M. Buisson and X. Chateau, *The European Physical Journal E*, 2015, **38**, 1–7.
14 N. Taccoen, F. Lequeux, D. Z. Gunes and C. N. Baroud, *Physical Review X*, 2016, **6**, 011010.
15 H. Xu, S. Melle, K. Golemanov and G. Fuller, *Langmuir*, 2005, **21**, 10016–10020.
16 M. Abkarian, A. B. Subramaniam, S.-H. Kim, R. J. Larsen, S.-M. Yang and H. A. Stone, *Physical review letters*, 2007, **99**, 188301.
17 S. Knoche, D. Vella, E. Aumaitre, P. Degen, H. Rehage, P. Cicuta and J. Kierfeld, *Langmuir*, 2013, **29**, 12463–12471.
18 P. J. Beltramo, M. Gupta, A. Alicke, I. Liascukiene, D. Z. Gunes, C. N. Baroud and J. Vermant, *Proceedings of the National Academy of Sciences*, 2017, 201705181.
19 F. X. Sicard and A. Striolo, *Nanoscale*, 2017.
20 T.-L. Cheng and Y. U. Wang, *Journal of colloid and interface science*, 2013, **402**, 267–278.
21 C. Gu and L. Botto, *Soft matter*, 2016, **12**, 705–716.
22 S. S. Datta, H. C. Shum and D. A. Weitz, *Langmuir*, 2010, **26**, 18612–18616.
23 P. Yue, J. J. Feng, C. Liu and J. Shen, *Journal of Fluid Mechanics*, 2004, **515**, 293–317.
24 Y. Tsuji, T. Kawaguchi and T. Tanaka, *Powder technology*, 1993, **77**, 79–87.
25 A. Di Renzo and F. P. Di Maio, *Chemical engineering science*, 2004, **59**, 525–541.
26 H. Zhu, Z. Zhou, R. Yang and A. Yu, *Chemical Engineering Science*, 2007, **62**, 3378–3396.
27 S. O'brien, *Journal of colloid and interface science*, 1996, **183**, 51–56.
28 O. Pitois and X. Chateau, *Langmuir*, 2002, **18**, 9751–9756.
29 R. Ettelaie and S. V. Lishchuk, *Soft Matter*, 2015, **11**, 4251–4265.
30 B. P. Binks and P. Fletcher, *Langmuir*, 2001, **17**, 4708–4710.
31 D. Jacqmin, *Journal of Computational Physics*, 1999, **155**, 96–127.
32 P. Yue, C. Zhou and J. J. Feng, *Journal of Fluid Mechanics*, 2010, **645**, 279–294.
33 V. Khatavkar, P. Anderson and H. Meijer, *Chemical engineering science*, 2006, **61**, 2364–2378.
34 P. Yue, C. Zhou, J. J. Feng, C. F. Ollivier-Gooch and H. H. Hu, *Journal of Computational Physics*, 2006, **219**, 47–67.
35 S. B. Pope, *Turbulent flows*, 2001.
36 G. Marsaglia *et al.*, *The Annals of Mathematical Statistics*, 1972, **43**, 645–646.
37 E. Aumaitre, S. Knoche, P. Cicuta and D. Vella, *EPL*, 2013.
38 W. T. Irvine, V. Vitelli and P. M. Chaikin, *Nature*, 2010, **468**, 947–951.
39 K. Stephenson, *Introduction to circle packing: The theory of discrete analytic functions*, Cambridge University Press, 2005.
40 N. Stoop, R. Lagrange, D. Terwagne, P. M. Reis and J. Dunkel, *Nature materials*, 2015, **14**, 337–342.
41 D. Vella, J. Bico, A. Boudaoud, B. Roman and P. M. Reis, *Proceedings of the National Academy of Sciences*, 2009, **106**, 10901–10906.
42 Y. Ebata, A. B. Croll and A. J. Crosby, *Soft Matter*, 2012, **8**, 9086–9091.
43 E. Hohlfeld and B. Davidovitch, *Physical Review E*, 2015, **91**, 012407.
44 G. Prabhudesai, I. Bihi, F. Zoueshtiagh, J. Jose and M. Baudoin, *Soft Matter*, 2017.
45 A. Vidal and L. Botto, *Journal of Fluid Mechanics*, 2017, **813**,

152–174.